Data evaluation of laminar flow diffusion chamber nucleation experiments with different computational methods

D. Mitrakos,[1,2] V. Ždímal,[3] D. Brus,[3,4] and C. Housiadas[1,a)]
[1]*"Demokritos" National Centre for Scientific Research, P.O. Box 60228, Agia Paraskevi, 15310 Athens, Greece*
[2]*Faculty of Mechanical Engineering, National Technical University of Athens, 15780 Athens, Greece*
[3]*Laboratory of Aerosol Chemistry and Physics, Institute of Chemical Process Fundamentals ASCR, v.v.i., Rozvojová 135, CZ-16502 Prague, Czech Republic*
[4]*Finnish Meteorological Institute, Erik Palménin aukio 1, P.O. Box 503, FI-00101 Helsinki, Finland*

(Received 3 April 2008; accepted 11 June 2008; published online 1 August 2008)

In order to evaluate the experimental data from laminar flow diffusion chamber (LFDC) experiments on homogeneous nucleation, an extensive postmeasurement computational analysis is required. The present work investigates the influence of the used computational methodology on the derived nucleation curves. To this end a reanalysis is made of previous LFDC experiments of 1-butanol nucleation in helium [D. Brus *et al.*, J. Chem. Phys. **122**, 214506 (2005)] using two different methods. The first method is based on single fluid heat and vapor transport in the carrier gas ignoring the aerosol processes, as commonly made in LFDC data evaluations. The second method is more comprehensive as is based on multidimensional computational fluid-particle dynamics. The calculations are made under the usual simplification of one-way coupling between fluid flow and particles, which is a valid approximation in most practical aerosols, while full aerosol dynamical effects are accommodated. Similar results were produced by the two methods. This finding corroborates the usual practice of omitting aerosol calculations in LFDC experimental data evaluation. © *2008 American Institute of Physics*. [DOI: 10.1063/1.2953330]

I. INTRODUCTION

The mechanisms of particle formation from a gas phase are of interest in many current applications. Industrial production of nanoparticles, climate change, or nuclear accident analysis are some examples from the diversity of fields where gas-to-particle conversion plays a major role. Particle formation often takes place via the mechanism of homogeneous nucleation, e.g., formation of embryo liquid droplets by condensation of vapor monomers. Many works, both theoretical and experimental, can be found in the literature on investigations of homogeneous nucleation. However, a satisfactory theory for a quantitative description of the homogeneous nucleation rate with macroscopic parameters is still not available. The most common experimental methods used for the measurement of the nucleation rate are the fast expansion cloud chamber,[1,2] the two piston expansion cloud chamber,[3,4] the shock tube,[5,6] the supersonic nozzle,[7] the thermal diffusion cloud chamber (TDCC),[8–15] and the laminar flow diffusion chamber (LFDC).[16–21]

The present work is concerned with the LFDC method. The LFDC method is currently gaining growing attention, not only for the experimental measurements of the nucleation rate but also as a method for the synthesis of high purity nanoparticles.[22] In the LFDC a gas carrying the vapor of interest is conducted into a cold tube ("the condenser"). The cooling of gas leads to supersaturation, giving rise to particle formation by homogeneous nucleation. The construction of LFDCs is simple because they usually operate at atmospheric pressure. Additionally, they achieve higher nucleation rates than TDCCs, thus offering the capability of investigating an expanded range of experimental parameters. The principal drawback of LFDCs is the need to employ complicated postprocessing numerical methods to evaluate the experimental data. Indeed, the experimental aim is to derive the nucleation rate J as a function of the saturation ratio S and temperature T. This is usually presented in the form of J-vs-S isotherms. In LFDC experiments nucleation occurs at an *a priori* unknown location between the inlet and the outlet of the condenser. The flow is thus divided into two zones, the upstream particle-free zone between the inlet and the nucleation location (single fluid flow), and the downstream particle-ladden zone between the nucleation location and the outlet (aerosol flow). Clearly J,S,T cannot be measured directly at the nucleation location. The rate J is extracted indirectly from the measurements of the particle number concentration at the condenser exit, whereas S and T at the location where the nucleation occurs are obtained through heat and mass transfer modeling.[17,23,24] Due to the extreme sensitivity of J on both S and T and the exponential dependence of S on T, a meticulous experimental control of temperatures and concentrations is required in LFDC experiments, as well as accurate and detailed postexperiment data evaluation with appropriate models. The significance of various experimental and modeling parameters and uncertainties on the evaluation of LFDC data has been examined in several works in the literature.[17–19,24–30] Despite, however, the

a)Author to whom correspondence should be addressed. Electronic mail: christos@ipta.demokritos.gr.

large number of LFDCs analyses presented in the literature, a more comprehensive analysis, allowing the determination of J,S,T from computational fluid-particle dynamics is still lacking. Generally, in all previous LFDC experiments S and T are derived by calculating heat and mass transfer in the upstream zone only, and J is obtained by using approximations based on similarity principles in the downstream zone, without taking into account the transport and dynamics of particles in this zone. An exception is the recent modeling work of Hermann *et al.*,[30] in which aerosol effects in LFDC operation are simulated by using a modal representation of the size distribution. The focus of the work is on the assessment of the capabilities of the software package FLUENT-FPM (fine particle mode) to simulate LFDC experiments.

In this work we present a reanalysis of previous LFDC experiments performed by some of the authors by using two different data evaluation modeling approaches. The experimental case reanalyzed is the homogeneous nucleation experiments of 1-butanol in helium.[24] The objective is to investigate whether more complicated and accurate modeling approaches can result in significantly different J-vs-S isotherms. The aim is to examine if the discrepancies observed in nucleation curves measured using different experimental techniques,[24] or even using the same experimental technique,[23,24] may be explained by the assumptions used in the data evaluation modeling methods.

The first method we use is similar to that commonly used in the data evaluation of such experiments (see, for example, the analysis that was used before in Ref. 24). Namely, the usual approximations are used in the downstream zone for the derivation of the maximum nucleation rate from the measured outlet particle number concentration,[31,32] whereas a single fluid heat and mass transfer analysis is performed in the upstream zone for the derivation of S and T. The second method is based on combined computational fluid dynamics (CFD) and aerosol dynamics calculations simulating the whole LFDC operation. For this purpose we performed multidimensional, sectional, fully Eulerian computational fluid-particle dynamics calculations based on a model recently developed by some of the authors.[33] The analysis is based on the usual approximation of one-way coupling between fluid and particles. This is not a serious limitation because in most practical aerosol cases, the coupling effects from the aerosol processes back into the fluid flow are insignificant. Therefore, the second method can be considered as quasiful comprehensive because it includes the aerosol dynamics analysis.

II. EXPERIMENT DESCRIPTION

The description of the LFDC has been previously presented in detail.[24] Here, only a brief summary of the experimental technique is given. The LFDC used in this investigation is based on a design of Lihavainen and Viisanen.[34] A schematic picture of the experimental apparatus is presented in Fig. 1. The LFDC consists of three main parts: a saturator, a preheater, and a condenser. Helium first enters the horizontal saturator containing liquid 1-butanol. At the exit of the saturator the gas is saturated with 1-butanol vapor. In the preheater, which is perpendicularly connected to the end of the saturator, the gas flow becomes parabolic. The vapor-gas mixture is then rapidly cooled in the condenser by heat exchange through the condenser wall. The temperature of the condenser is much lower than that of the saturator and hence supersaturation is obtained, leading to particle formation by homogeneous nucleation. Heat diffuses faster than mass in the 1-butanol-helium mixture (Lewis number equal to 5.8, greater than 1), and so a well-defined nucleation zone is produced in the center of the tube.

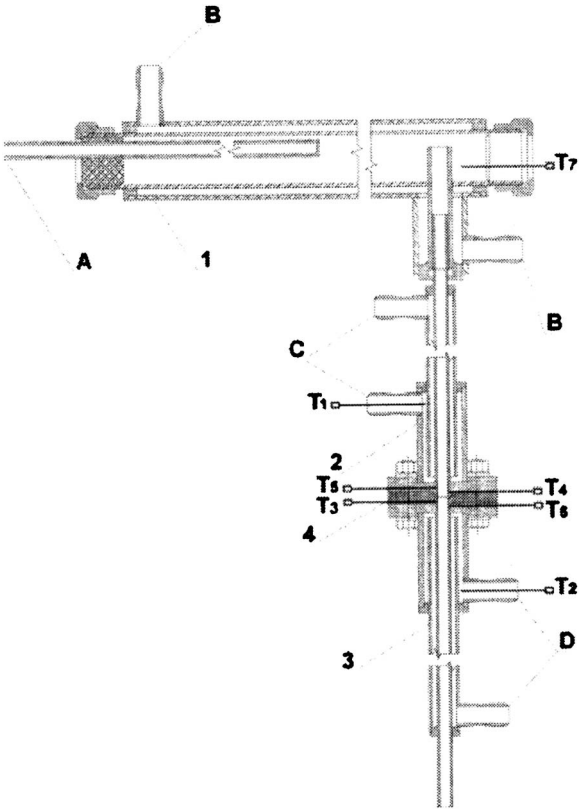

FIG. 1. Schematic picture of the LFDC. (1) Saturator, (2) preheater, (3) condenser, (4) Teflon spacer, (A) carrier gas inlet, (B) saturator thermostated liquid inlet and outlet, (C) preheater thermostated liquid inlet and outlet, and (D) condenser thermostated liquid inlet and outlet, T1–T7: thermocouples.

The concentration of the vapor in the mixture is controlled by the saturator temperature. The gas flow was carefully chosen to ensure the proper operation of the saturator. The level of supersaturation is controlled by the temperature difference between the saturator and the condenser, while the nucleation temperature is controlled by the temperatures of the preheater and the condenser. The entering flow of helium is filtered by a high efficiency particle absorber to avoid possible heterogeneous nucleation. The gas flow rate is controlled by a mass flow controller and checked with a soap bubble flow calibrator. The preheater and the condenser are separated by a Teflon spacer, in order to achieve a steep temperature drop in the transition zone. The saturator temperature is measured at one point, and the temperatures in the preheater and the condenser are measured at six locations, with chromel-allumel thermocouples. The particles formed are counted optically by a system consisting of a small diode

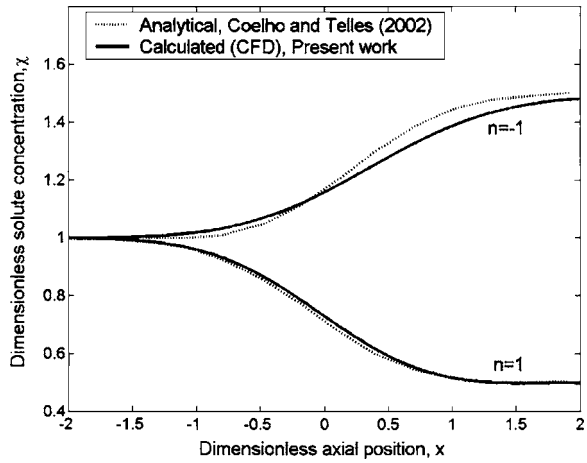

FIG. 2. Dimensionless solute concentration at the upper ($n=1$) and lower ($n=-1$) plates as a function of the dimensionless axial position, as calculated with the CFD code, in comparison with the analytical results, as reported in Fig. 4 of Coehlo and Telles (Ref. 38).

laser including a beam shaping lens, a photomultiplier tube, and electronics for discrimination and counting.

III. DATA EVALUATION MODELING METHODS

A. Method 1: CFD in the upstream zone

In this approach the steady state temperature and vapor concentration profiles in the upstream zone of the chamber are calculated by solving the Navier–Stokes equations, the energy equation (convective heat transfer), and the species transport equation (convective mass transfer) with a commercial, general purpose CFD package.[35] The thermal diffusion (Soret effect), i.e., vapor diffusion in the gas induced by the temperature gradient,[36,37] is taken into account. The species transport equation is therefore given by

$$\nabla \cdot (\rho \mathbf{u} C_m) - \nabla \cdot (\rho D_v \nabla C_m) = \nabla \cdot \left(\alpha D_v \rho C_m \left(\frac{1}{T} \right) \nabla T \right). \tag{1}$$

In the above equation C_m is the species mass fraction, $\mathbf{u}$ is the gas velocity vector, D_v is the binary diffusion coefficient of the vapor in the gas, ρ is the density of the gas, α is the thermal diffusion factor, and T is the temperature.

The Soret effect [term on the right-hand side of Eq. (1)] is accommodated in the CFD calculations by means of a user-specified source term. In order to check whether the Soret effect was implemented correctly, we made comparisons with the analytical solution of Coelho and Silva Telles.[38] These authors recently reported results for simultaneous heat and mass transfer in a binary fluid flow, between two unevenly heated plates, taking into account the effect of temperature gradient on the solute mass transfer. In Fig. 2 the dimensionless solute concentrations along the dimensionless axial position for the upper ($n=1$) and lower ($n=1$) plates are shown, as calculated with the CFD code, and in comparison with the analytical results. Excellent agreement is observed for the upper plate. The agreement for the lower plate is less favorable but still very good, considering the errors in the numerical evaluation of the analytical solution because of the presence, in this case, of many high order polynomials (personal communication with Coelho and Telles). We can conclude that the Soret effect was implemented properly in the CFD calculations.

Besides including carefully the Soret effect in our CFD calculations, we also paid attention to use accurate wall temperature boundary conditions. The influence of boundary conditions may be significant in LFDC calculations.[27,28] Instead of approximating the wall temperature by an idealized axial step, as in the original analysis of Brus *et al.*,[24] we used the wall temperature profiles, as measured in the experiments. Note also that in the original analysis of Brus *et al.*,[24] the saturation ratio and temperature profiles in the condenser are calculated by solving the two-dimensional energy and vapor mass equations only. The gas momentum and continuity equations are not solved. Instead, the gas velocity is taken to be parabolic, assuming a constant gas density, calculated at the average temperature of the preheater and the condenser. In the present approaches the gas velocity fields are determined by means of a CFD analysis solving the coupled heat and momentum transfer problems and using temperature-dependent properties.

With known temperature and vapor concentration profiles in the upstream zone of the condenser, the theoretical nucleation rate profiles J_{the} are then estimated by using the classical nucleation theory. The location where J_{the} reaches a maximum and the corresponding values of T and S are then determined. The experimental nucleation rate J_{expt} is estimated from the relationship proposed by Wagner and Anisimov[32] as follows:

$$\frac{J_{\text{expt}}}{\dot{V} N_{\text{out}}} = \frac{J_{\text{the}}^{\max}}{\int J_{\text{the}} dV}, \tag{2}$$

where N_{out} is the measured particle number concentration at the outlet, V is the volumetric flow rate, and $\int J_{\text{the}} dV$ is the theoretical nucleation rate integrated over the volume of the nucleation region. We note that the experimental nucleation rate derived from Eq. (2) is relatively independent of the theory chosen to evaluate the right-hand side, as shown in Refs. 17 and Ref. 31.

B. Method 2: Multidimensional CFD-based aerosol model

This method is based on a multidimensional aerosol dynamics analysis, performed using a sectional, CFD-based aerosol model recently developed by the authors.[33] The temporal and spatial variations of the particulate phase and the condensable vapor phase inside the reactor are described by the general dynamic equation and the condensable vapor transport equation, respectively. These two governing equations can be written as follows:

$$\frac{\partial \rho n_m}{\partial t} + \nabla \cdot (\rho (\mathbf{u} + \mathbf{c}_{\text{th}}) n_m) - \nabla \cdot (\rho D_p \nabla n_m) = \left. \frac{\partial \rho n_m}{\partial t} \right|_{\text{nucl}} + \left. \frac{\partial \rho n_m}{\partial t} \right|_{\text{growth}} + \left. \frac{\partial \rho n_m}{\partial t} \right|_{\text{coag}}, \tag{3}$$

$$\frac{\partial \rho C_m}{\partial t} + \nabla \cdot (\rho \mathbf{u} C_m) - \nabla \cdot (\rho D_v \nabla C_m) = -\left.\frac{\partial \rho C_m}{\partial t}\right|_{\text{nucl}} - \left.\frac{\partial \rho C_m}{\partial t}\right|_{\text{growth}} + \left.\frac{\partial \rho C_m}{\partial t}\right|_{\text{Soret}}. \quad (4)$$

In Eq. (3) n_m is the particle size distribution function, expressed per unit mass of gas, i.e., number of particles per micrometer of size internal per kilogram of gas, $\mathbf{c}_{\text{th}}$ is the thermophoretic velocity of particles (vector), and D_p is the particle diffusion coefficient. The first, second, and third terms on the right-hand side of Eq. (3) represent the variation of the particle size distribution due to homogeneous nucleation, condensational growth, and coagulation, respectively. In Eq. (4) C_m is the vapor mass fraction, whereas the first and second terms on the right-hand side stand for the depletion of vapor due to homogeneous nucleation and condensational growth, respectively. The last term in Eq. (4) represents thermal diffusion (Soret effect).

The multidimensional aerosol dynamics calculation, described by the system of Eqs. (3) and (4), is one way coupled with the calculation of the gas temperature field and the velocity field inside the reactor. These fields are provided by the numerical solution of Navier–Stokes equations and the energy equation (convective heat transfer). The calculations are carried out with the CFD code ANSWER. The whole computation of the combined fluid and particle dynamics is carried out in two steps. First CFD calculations are made to determine the gas velocity and temperature fields in the condenser. These fields are then used as input to the aerosol dynamics calculations. The spatial CFD and aerosol dynamics grids are independent. The temperature and the gas velocity at the aerosol dynamics grid nodes are calculated by multidimensional linear interpolation[39] on the output data provided by the CFD calculations. Detailed description of the model and the numerical techniques used for the solution can be found elsewhere.[33]

C. Grid sizes and boundary conditions

The CFD runs are made in a two-dimensional uniform grid in cylindrical coordinates, consisting of 1000 axial and 30 radial nodes, assuming symmetry with respect to the condenser axis. The inlet of the computational domain is taken to be the outlet of the preheater (T5 in Fig. 1), where cooling of the wall begins. The temperature of the chamber wall is measured at four axial positions in the transition zone (the zone between the preheater and the condenser). The boundary temperature values at the wall nodes are assigned on the basis of a cubic spline interpolation on the measured temperature values. The inlet gas temperature is taken equal to that of the preheater. The flow inside the chamber is laminar. The preheater is long enough so the flow can be considered as fully developed at the inlet of the computational domain (parabolic velocity profile). For both methods the vapor mass fraction at the inlet is equal to that of the saturator. Vapor concentration at the wall is taken equal to the equilibrium value at the wall temperature. In a short zone downstream the entrance of the transition zone, the wall temperature is still higher than the saturator temperature. Therefore, the equilibrium vapor mass fraction at the wall temperature becomes higher than the inlet vapor mass fraction. The wall is taken adiabatic wherever $T_w > T_s$ in order to prevent the unphysical behavior of a vapor flux from the wall toward the gas stream. For the aerosol dynamics calculations the boundary condition for the particulate phase is to set the number density equal to zero at the inlet and at the wall (perfectly absorbing boundary).

The aerosol dynamics grid is also two dimensional, cylindrical, and symmetric about the condenser axis. The grid consists of 601 axial and 31 radial nodes, nonuniform at the axial direction (grid sizes ranging from about 0.25 mm in the transition zone to 2 mm elsewhere).

TABLE I. Ratios of experimental nucleation rates to the rates predicted by the classical nucleation theory, derived from the two methods, for each isotherm and comparison with the ratios of Brus *et al.* (Refs. 24 and 42).

Isotherm (K)	Method 1	Method 2	[a]
265	0.9–7.5	4.1	0.08–1.0
270	2.9–5.6	7.0	0.2–2.5
275	6.5–12.6	9.8	0.7–4.3
280	3.6–11.3	4.4	1.41–4.96

[a]Brus *et al.* (Refs. 24 and 42).

IV. RESULTS

Four sets of experimental measurements have been performed, each of them corresponding to a different *J*-vs-*S* isotherm. Each isotherm consists of a series of experiments, each of them corresponding to a different saturator temperature or, equivalently, to a different inlet vapor concentration (see Ref. 24). All four test series are reanalyzed, using the two different data evaluation methods presented in the previous section.

Table I compares the two methods in terms of the ratio of the experimental to the theoretical nucleation rate. This ratio corresponds to the correction factor, widely employed in the aerosol calculations, in order to get an agreement between the calculated and measured particle number concentrations.[21,28,33,40,41] In the present aerosol calculations, the correction was determined for each isotherm separately and kept the same in the runs for all the experiments belonging to the isotherm. For method 2, the variation of the correction factor between the isotherms is mild (within a factor of 2) and can be considered insignificant for this type of calculations. The ratios of the experimental to the theoretical nucleation rate, as calculated from method 1, are in close agreement with the correction factors used in method 2, and do not, also, vary significantly between the isotherms. For comparison, the ratios reported by Brus *et al.*[24] are also given in Table I, as calculated recently following a mistake found in the first analysis.[42] These ratios exhibit a similar, weak temperature dependency comparable with that of methods 1 and 2, although their values are generally reduced (shifted by less than one order of magnitude). Yet, methods 1 and 2 yielded correction factors of similar magnitude, with differences that can be considered as trivial for this type of calculations. Moreover, for both methods a constant correction

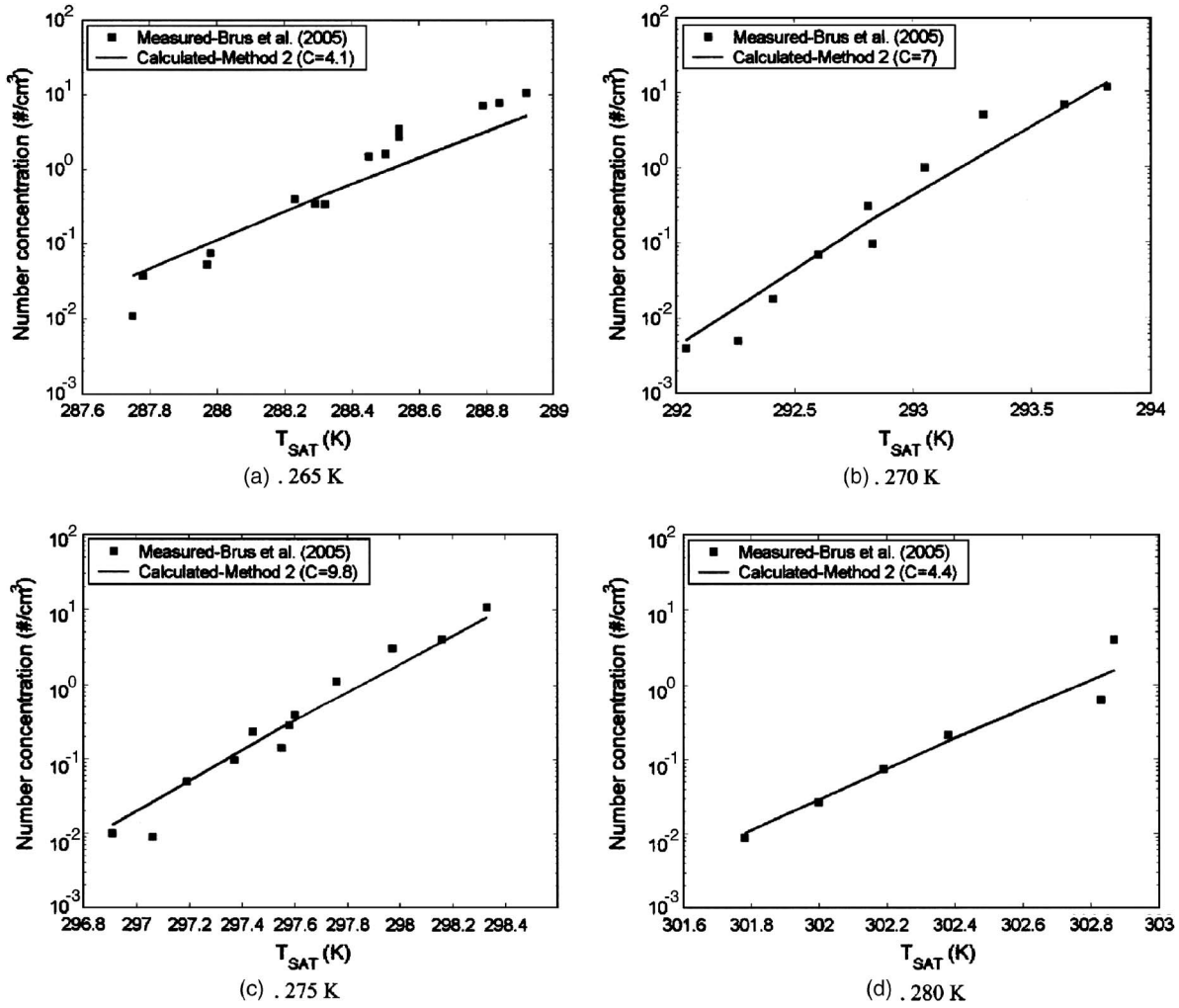

FIG. 3. Number concentrations at the exit of the condenser for the four different isotherms as calculated with method 2 and comparison with the experimental data.

factor could be used for each isotherm and this factor did not vary very much between isotherms (i.e., quasi-temperature-independent).

The bulk average particle number concentration at the exit of the condenser for each isotherm, as a function of the saturator temperature, as calculated with method 2 is shown in Figs. 3(a)–3(d), in comparison with the measured data. It can be observed that the model reproduces satisfactorily the dependence of measured data on the temperature of the saturator. Some small differences are observed between the calculated and the measured data that are attributed to the constant correction used for each isotherm. These differences, however, are insignificant considering the dispersion of the experimental results and the experimental uncertainties.

Figure 4 shows the *J*-*S* isotherms, as evaluated with the two computational methods. For comparison the results of the previous analysis of the experiments[24] are also shown, as recently reported in an erratum note on the original paper.[42] The isotherms found with the TDCC technique are also shown. A reasonable agreement is observed between the isotherms determined by method 1 and the corrected analysis of Brus *et al.*[42] at temperatures of 280 and 275 K. For the lower isotherms of 265 and 270 K, there is a significant discrepancy. The general trend is a shift to the left with our method 1, i.e., toward lower saturation ratios. The differences in the calculated saturation ratios can be attributed to the use of different boundary conditions for the temperature of the

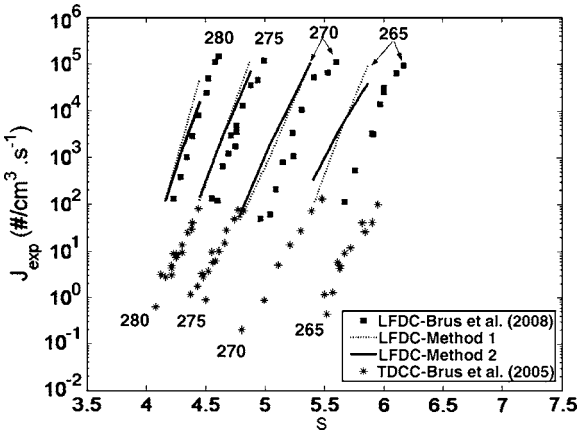

FIG. 4. The isothermal nucleation rates of 1-butanol as a function of its saturation ratio as produced by the two different computational methods. The original LFDC experimental data of Brus *et al.* (Ref. 24) are also shown [as reported in the erratum, see Brus *et al.* (Ref. 42)], as well as the TDCC experimental data.

chamber wall. It is worth noting that the present refined reanalysis as well as the corrected analysis of Brus *et al.*[42] permitted to reduce the initial discrepancies between the isotherms obtained with the LFDC and the TDCC by about one order of magnitude. Still, however, the remaining differences are not explained by the uncertainties introduced by the computational data evaluation methods.

From Fig. 4 we can also observe that the isotherms generated with the full aerosol model approach (method 2) are practically the same as those generated with the widely employed approximate approach (method 1). Consequently, the vapor mass transport in the chamber is not affected very much by the aerosol processes, i.e., the depletion of vapor due to homogeneous nucleation and particle growth by condensation is not important. This is due to the low nucleation rates and the resulting low particle number concentration. Some small differences can be observed regarding the range of the nucleation rate and the slope of the isotherms between methods 1 and 2. Inclusion of coagulation, diffusion, and thermophoretic deposition in method 2 explains part of the observed differences. However, the observed differences, which are also reflected in the calculation of the number concentration with method 2 [Figs. 3(a)–3(d)], are mostly numerical because they arise from the differences in the nucleation rate correction factors used in the runs of each method.

V. CONCLUSIONS

In this work we used two different modeling methods to evaluate the data of homogeneous nucleation experiments in LFDCs. The aim was to investigate the influence of the employed modeling approach on the derived results and, in particular, to find out whether more rigorous and comprehensive models are able to explain the serious discrepancies observed in the nucleation curves inferred from different experimental techniques. The first method is similar to that commonly used in LFDC experiments. Specifically, method 1 is based on single fluid heat and vapor transport in the zone upstream of the nucleation front, while the aerosol processes in the downstream zone are not modeled. Method 2 uses multidimensional CFD combined with aerosol dynamics modeling. The model that is used for this purpose is one way coupled since it does not take into account the influence of the aerosol processes on the fluid flow calculations, i.e., heat releases from aerosol formation and changes to the physical properties of the gas mixture. This is however a reasonable assumption for this kind of experiments, and so, this method can be considered as comprehensive, as it includes the calculation of the aerosol processes in the downstream zone.

From the obtained results the following conclusions can be drawn.

(a) The more comprehensive method 2 was found to require only slight corrections to the theoretical nucleation rates. The used correction factors can be considered as trivial for this type of calculations (less than 10). Moreover, they were found to exhibit a rather insignificant variation between the different nucleation isotherms. Therefore, multidimensional CFD-based aerosol modeling permits us to simulate the whole LFDC operation with good accuracy.

(b) The ratios of the experimental to theoretical nucleation rates, as derived from method 1, were found to remain the same between the different isotherms and in close agreement with the correction factors used in method 2. Also, similar results were produced by methods 1 and 2 in terms of the nucleation rate (J) versus saturation ratio (S) isotherms. These findings validate the usual practice of omitting aerosol calculations in LFDC experimental data evaluation.

(c) From the practical point of view, method 1 is preferable to method 2 because it requires significantly lower development and computational effort. However, in implementing method 1 caution is required in describing as precisely as possible fluid flow, heat transfer, and vapor transfer. The J-S isotherms produced with refined modeling are shifted closer to the isotherms established from TDCC experiments. However, the use of more rigorous modeling assumptions alone does not explain the discrepancies between the nucleation curves obtained with different experimental techniques.

ACKNOWLEDGMENTS

This work was supported partially by GSRT (General Secretariat of Research and Technology) in the framework of a bilateral (Hellenic Rep., Czech Rep.) Scientific and Technical cooperation project and partially by the Ministry of Education, Youth and Sports of the Czech Republic, Grant No. ME699.

[1] R. C. Miller, R. J. Anderson, and J. L. Kassner, Jr., in *Colloid and Interface Science* (Academic, New York, 1976), Vol. II, p. 1.
[2] J. L. Schmitt, G. W. Adams, and R. A. Zalabsky, J. Chem. Phys. **77**, 2089 (1982).
[3] P. E. Wagner and R. Strey, J. Phys. Chem. **85**, 2694 (1981).
[4] R. Strey, P. E. Wagner, and Y. Viisanen, J. Chem. Phys. **98**, 7748 (1994).
[5] F. Peters, J. Chem. Phys. **77**, 4788 (1982).
[6] K. N. H. Loojimans, P. C. Kreisels, and M. E. H. van Dongen, J. Chem. Phys. **106**, 4152 (1993).
[7] Y. J. Kim, B. E. Wyslouzil, G. Wilemski, J. Wölk, and R. Strey, J. Phys. Chem. **108**, 4365 (2004).
[8] J. L. Katz and B. J. Ostermier, J. Chem. Phys. **47**, 478 (1976).
[9] R. H. Heist and H. Reiss, J. Chem. Phys. **59**, 665 (1973).
[10] J. Smolik and J. Vitovec, Collect. Czech. Chem. Commun. **41**, 1471 (1976).
[11] C. Becker, H. Reiss, and R. H. Heist, J. Chem. Phys. **68**, 3585 (1978).
[12] C. Flageollet-Daniel, P. Erhard, and P. Mirabel, J. Chem. Phys. **75**, 4615 (1981).
[13] C.-H. Hung, M. J. Krasnopoler, and J. L. Katz, J. Chem. Phys. **90**, 1856 (1989).
[14] G.-S. Cha, H. Uchtmann, J. A. Fisk, and J. L. Katz, J. Chem. Phys. **101**, 459 (1994).
[15] J. Smolik and V. Ždímal, Aerosol Sci. Technol. **20**, 127 (1994).
[16] M. P. Anisimov and A. Cherevko, J. Aerosol Sci. **16**, 97 (1985).
[17] K. Hämeri and M. Kulmala, J. Chem. Phys. **105**, 7696 (1996).
[18] V. Vohra and R. H. Heist, J. Chem. Phys. **104**, 382 (1996).
[19] V. B. Mikheev, N. S. Laulainen, S. E. Barlow, M. Knott, and I. J. Ford, J. Chem. Phys. **113**, 3704 (2000).
[20] H. Lihavainen, Y. Viisanen, and M. Kulmala, J. Chem. Phys. **114**, 10031 (2001).
[21] H. V. Nguyen, K. Okuyama, T. Mimura, Y. Kousaka, R. C. Flagan, and J. H. Seinfeld, J. Colloid Interface Sci. **119**, 491 (1987).

[22] U. Backman, J. K. Jokiniemi, A. Auvinen, and K. E. J. Lehtinen, J. Nanopart. Res. **4**, 325 (2002).
[23] H. Lihavainen, Ph.D. thesis, Finnish Association for Aerosol Research, 2000.
[24] D. Brus, A. P. Hyvärinen, V. Ždimal, and H. Lihavainen, J. Chem. Phys. **122**, 214506 (2005).
[25] S. P. Fisenko and A. A. Brin, Int. J. Heat Mass Transfer **49**, 1004 (2006).
[26] C. Housiadas, E. Papanicolaou, and Y. Drossinos, J. Aerosol Sci. **33**, 797 (2002).
[27] C. Housiadas, F. Ezquerra Larrode, and Y. Drossinos, J. Aerosol Sci. **31**, 959 (2000).
[28] M. Wilck and F. Stratmann, J. Aerosol Sci. **28**, 959 (1997).
[29] A.-P. Hyvärinen, D. Brus, V. Ždímal, J. Smolík, M. Kulmala, Y. Viisanen, and H. Lihavainen, J. Chem. Phys. **124**, 224304 (2006).
[30] E. Herrmann, H. Lihavainen, A.-P. Hyvärinen, I. Riipinen, M. Wilck, F. Stratmann, and M. Kulmala, J. Phys. Chem. A **110**, 12448 (2006).
[31] M. P. Anisimov, K. Hämeri, and M. Kulmala, J. Aerosol Sci. **25**, 23 (1994).
[32] P. E. Wagner and M. P. Anisimov, J. Aerosol Sci. **24**, S103 (1993).
[33] D. Mitrakos, E. Hinis, and C. Housiadas, Aerosol Sci. Technol. **41**, 1076 (2007).
[34] H. Lihavainen and Y. Viisanen, J. Phys. Chem. B **105**, 11619 (2001).
[35] ANSWER User's Manual (Analytic & Computational Research, Bel Air, CA, 2001).
[36] S. Chapmann and T. G. Cowling, *The Mathematical Theory of Non-Uniform Gases* (Cambridge University Press, Cambridge, 1970).
[37] J. O. Hirschfelder, C. F. Curtiss, and R. B. Bird, *The Molecular Theory of Gases and Liquids* (Wiley, New York, 1964).
[38] R. M. L. Coelho and A. Silva Telles, Int. J. Heat Mass Transfer **45**, 3101 (2002).
[39] W. H. Press, S. A. Teukolsky, W. T. Vetterling, and B. P. Flannery, *Numerical Recipes in Fortran: The Art of Scientific Computing*, 2nd ed. (Cambridge University Press, Cambridge, 1994).
[40] G. M. Phanse and S. E. Pratsinis, Aerosol Sci. Technol. **11**, 100 (1989).
[41] J. Pyykönen and J. Jokiniemi, J. Aerosol Sci. **31**, 531 (2000).
[42] D. Brus, A.-P. Hyvärinen, V. Ždímal, and H. Lihavainen, J. Chem. Phys. **128**, 079901 (2008).